NEUROSCIENCE

The omega-3 hydroxy fatty acid 7(*S*)-HDHA is a high-affinity PPARα ligand that regulates brain neuronal morphology

Jiabao Liu[1], Cigdem Sahin[2], Samar Ahmad[3], Lilia Magomedova[2], Minhao Zhang[4], Zhengping Jia[5,6], Adam H. Metherel[7], Arturo Orellana[4], Gennady Poda[2,8], Richard P. Bazinet[7], Liliana Attisano[3], Carolyn L. Cummins[2], Hui Peng[9,10]*, Henry M. Krause[1,11]*

The nuclear receptor peroxisome proliferator-activated receptor alpha (PPARα) is emerging as an important target in the brain for the treatment or prevention of cognitive disorders. The identification of high-affinity ligands for brain PPARα may reveal the mechanisms underlying the synaptic effects of this receptor and facilitate drug development. Here, using an affinity purification–untargeted mass spectrometry (AP-UMS) approach, we identified an endogenous, selective PPARα ligand, 7(*S*)-hydroxy-docosahexaenoic acid [7(*S*)-HDHA]. Results from mass spectrometric detection of 7(*S*)-HDHA in mouse and rat brain tissues, time-resolved FRET analyses, and thermal shift assays collectively revealed that 7(*S*)-HDHA potently activated PPARα with an affinity greater than that of other ligands identified to date. We also found that 7(*S*)-HDHA activation of PPARα in cultured mouse cortical neurons stimulated neuronal growth and arborization, as well as the expression of genes associated with synaptic plasticity. The findings suggest that this DHA derivative supports and enhances neuronal synaptic capacity in the brain.

INTRODUCTION

Nuclear receptors are a class of ligand-regulated transcription factors that are bound and regulated by endogenous or exogenous lipophilic molecules, including hormones, vitamins, and dietary lipids. Nuclear receptors directly regulate target gene expression, thereby coordinating a variety of biological processes, including reproduction, development, and metabolism (*1*, *2*). Peroxisome proliferator-activated receptor alpha (PPARα) is a nuclear receptor family member that is widely expressed (*3*, *4*), responds to variations in available free fatty acids, and accelerates or decelerates fatty acid metabolism accordingly. In the liver, it is a key regulator of fatty acid oxidation (*5*), ketogenesis, lipid transport, metabolism, and gluconeogenesis (*6*, *7*). PPARα is also expressed in all regions of the adult brain (*8*), where it is involved in neural cell differentiation and death as well as in inflammation and neurodegeneration (*9*, *10*). Activation of PPARα can also prevent amyloid beta (Aβ) peptide overproduction and accumulation by up-regulating neuronal expression of the cell surface protease A disintegrin and metalloproteinase 10 (ADAM10) (*11*). Pharmacological activation of PPARα in a mouse model of Alzheimer's disease decreases amyloid plaque pathology and reverses memory deficits (*12*). It has also been shown that PPARα has a role in regulating hippocampal plasticity through transcriptional up-regulation of adenosine 3′,5′-monophosphate (cAMP)–response element-binding protein (CREB) (*13*). Notably, activation of PPARα in quiescent adult hippocampal neural stem/progenitor cells also promotes hippocampal neurogenesis (*14*). In addition, mouse and human genetic studies suggest a role for PPARα in reducing susceptibility to schizophrenia (*15*–*17*). Thus, PPARα has the potential to prevent or reverse neurological pathologies through multiple pathways.

A number of endogenous lipids have been shown to act as PPARα ligands in cell culture. These include phosphocholine [1-palmitoyl-2-oleoyl-sn-glycero-3-phosphocholine (GPC)] (*18*), specific monounsaturated fatty acids [oleic acid (OA) and petroselinic acid] (*19*), some polyunsaturated fatty acids such as arachidonic acid (AA) and metabolites of AA such as 8-hydroxy-eicosatetraenoic acid (8-HETE) (*19*), and leukotriene B4 (LTB4) (*20*). Although these ligands can activate PPARα in cultured cells, their affinities for PPARα are all relatively low [>10 μM median effective concentration (EC_{50})], raising concerns that they may not be relevant PPARα regulators in vivo.

The signaling pathways of PPARα in the brain are quite different from those in metabolic tissues (*21*). The composition and abundance of the brain lipids that are required to maintain brain structural integrity are also very different from those that predominate in metabolic tissues such as the liver and adipose, where they are used primarily for energy use or storage (*22*). The blood-brain barrier also blocks the passage of major lipid carriers such as lipoproteins and albumin, as well as nonessential fatty acids in the blood (*22*). Together, these differences suggest the possible existence of tissue-selective PPARα ligands, target genes, and associated functions in the brain. Thus, much of the extensive information gleaned from studies of PPARα ligands and functions in metabolic tissues may have little relevance in the brain. Consistent with these suggestions, new brain-specific fatty acyl amides with the ability to regulate PPARα activity have been found in the brain. These include hexadecanamide (HEX), 9-octadecenamide (OCT) (*23*), and oleoylethanolamide (OEA) (*24*). However, the affinities of these molecules for PPARα are also low, and their levels of abundance in the brain have not been reported.

[1]Donnelly Centre for Cellular and Biomolecular Research, University of Toronto, Toronto, ON M5S 3E1, Canada. [2]Department of Pharmaceutical Sciences, University of Toronto, Toronto, ON M5S 3M2, Canada. [3]Department of Biochemistry, University of Toronto, Toronto, ON M5S 3E2. [4]Department of Chemistry, York University, Toronto, ON M3J 1P3, Canada. [5]Neurosciences and Mental Health, The Hospital for Sick Children, Toronto, ON M5G 1X8, Canada. [6]Department of Physiology, University of Toronto, Toronto, ON M5S 1A8, Canada. [7]Department of Nutritional Sciences, Faculty of Medicine, University of Toronto, Toronto, ON, Canada. [8]Drug Discovery, Ontario Institute for Cancer Research, Toronto, ON M5G 0A3, Canada. [9]Department of Chemistry, University of Toronto, Toronto, ON M5S 3H6, Canada. [10]School of the Environment, University of Toronto, Toronto, ON M5S 3H6, Canada. [11]Department of Molecular Genetics, University of Toronto, Toronto, ON M5S 1A8, Canada.
*Corresponding author. Email: h.krause@utoronto.ca (H.M.K.); hui.peng@utoronto.ca (H.P.)

One of the more abundant brain lipids, docosahexaenoic acid (DHA), is an ω-3 polyunsaturated fatty acid that constitutes as much as 30 to 40% of the brain's total polyunsaturated fatty acid content (*25*) but only about 10 to 15% of cortex total fatty acids (*26*). DHA has been shown to accumulate preferentially in brain regions that are involved in memory and attention, such as the cerebral cortex and hippocampus (*27*, *28*). Evidence from numerous human and animal studies, from infant to adult, indicates that DHA is correlated with brain development and cognition (*29*–*31*). Studies also suggest that DHA deficiency is associated with increased risk of schizophrenia and neurodegenerative diseases (*15*, *32*). Despite these findings though, uncertainties remain regarding the benefits of DHA supplementation in adults (*33*–*35*).

Here, using affinity pull-downs and untargeted mass spectrometry, we found that a DHA-derived molecule, 7(*S*)-hydroxy-docosahexaenoic acid [7(*S*)-HDHA], is a physiological ligand for PPARα. We show that 7(*S*)-HDHA is the highest-affinity endogenous ligand for PPARα identified in brain thus far, with its relatively high affinity due in part to an ability to interact uniquely with an additional Cys residue in the ligand binding pocket. In mouse cortical neurons, we show that 7(*S*)-HDHA promotes multiple dendritic responses at physiologically relevant concentrations. We also find that supplementation of DHA further increases the endogenous levels of 7(*S*)-HDHA in rat cortex, suggesting a possible mechanism for DHA action via conversion to 7(*S*)-HDHA and PPARα activation.

RESULTS

Affinity pull-downs identify 7(*S*)-HDHA as a PPARα ligand

To identify relevant and high-specificity ligands for PPARα in the brain, we developed an affinity pull-down method for selectively capturing high-affinity PPARα ligands from tissue extracts (fig. S1A). A His-tagged human PPARα ligand binding domain (LBD) construct was used as bait to fish out relatively low abundance, but high-affinity endogenous ligands present in total metabolites extracted from dissected brain tissues. A magnetic bead–based affinity step was optimized for the pull-downs, followed by a fast size exclusion chromatography step to remove additional nonspecifically associated lipids. Bound ligands were then separated from the receptor and analyzed by untargeted metabolomics using liquid chromatography–mass spectrometry (LC-MS). Nonspecific and low-affinity interactions were further minimized by comparing identified masses with components purified using other receptors (fig. S1A). To benchmark the approach, we tested the method with multiple receptors [PPARα, PPARβ, PPARγ, retinoic acid receptor (RAR)-related orphan receptor-alpha (RORγ), and farnesoid X receptor (FXR)] together with known ligands, spiked together at 100 nM into our lipid extracts (fig. S1, B to D). The optimized method was found to be highly selective as evidenced by the specific pull-downs mediated by each of the tested receptors. In each case, an average signal-to-noise ratio of >10,000 was achieved for all ligands tested.

We then applied this approach to screen our PPARα-LBD construct against brain anatomical lipid extracts, using the PPARβ-LBD construct as a negative control, and with each receptor pull-down performed in triplicate. Two mass features [mass/charge ratio (*m/z*) = 343.2274 and 344.2307] were consistently and selectively enriched from mouse hippocampus samples by the PPARα-LBD ($P = 0.0001$, 417-fold enrichment, and $P = 0.0002$, 98-fold enrichment, respectively) using ESI^- mode LC-MS (Fig. 1A and table S1). Both masses were subsequently assigned as isotopic peaks of a hydroxylated isoform of an omega-3 hydroxy fatty acid (ω-3 HFA) according to predicted elemental compositions [$(C_{22}H_{31}O_3)^-$, $\Delta m = -1.4$ parts per million (ppm)]. This HDHA isoform was also detected as the top hit ($P = 0.00003$ and 1372-fold enrichment) in the PPARα pull-down sample obtained under ESI^+ ionization (*m/z* 327.2310, $[M + H - H_2O]^+$) (Fig. 1B and table S1). The same ions were subsequently detected in PPARα pull-downs using mouse cortex ($P = 0.0003$, 23-fold enrichment at negative mode, and $P = 0.0015$, 182-fold enrichment at positive mode) (Fig. 1, C and D) and cerebellum extracts (table S1). MS^2 analysis assigned this compound as 7-HDHA, with two fragments (*m/z* = 141.0548 and 113.0596, calc for $[C_7H_9O_3]^-$ and $[C_6H_9O_2]^-$, respectively, $\Delta m = -2.8$ ppm) (Fig. 1E) cleaved at the C_7-C_8 and C_6-C_7 positions, respectively (Fig. 1F). The identity of 7-HDHA was further confirmed by comparing retention times (Fig. 2A) and MS^2 spectra (Fig. 1E) to a purchased 7-HDHA standard. To confirm the specificity of 7-HDHA as a PPARα ligand, we then tested for binding to other nuclear receptors. As observed above with PPARβ (Fig. 2B), 7-HDHA was also not pulled down by estrogen-related receptor-gamma (ERRγ), neuron-derived orphan receptor-1 (NOR1), or nuclear receptor related 1 (NURR1) (fig. S2), further suggesting that 7-HDHA is a selective ligand for PPARα. We did find detectable levels of 7-HDHA in PPARγ pull-downs (Fig. 2C), but unlike PPARα, PPARγ also pulled down most other HDHA isomers and many other hydroxy fatty acids. Experiments below also indicate that 7-HDHA is a much lower-affinity ligand for PPARγ than PPARα.

HDHAs are derived from the most abundant ω-3 FA in the brain, DHA. Previous studies have indicated that 4-, 11-, 14, and 20-HDHA are the most abundant isomers in brain, with previously detected levels four- to sixfold higher than 7-HDHA (*36*, *37*). Two ω-3 FAs, 4-HDHA and 17-HDHA, have also previously been shown to bind PPARγ (*38*). To check whether 4-, 17-HDHA, or other HDHAs were not pulled down by PPARα because of their absence in our extracts, we checked for their presence by LC-MS. As noted previously, all of the common HDHA isomers, including 4- and 17-HDHA, were present at similar or higher levels to 7-HDHA in crude brain extracts (Fig. 2D). Thus, our selective pull-down of only 7-HDHA by PPARα indicates that it is highly selective for this hydroxy isoform.

We also investigated whether other previously published PPARα ligands were present in our extracts. HETEs, metabolites of AA, are the most widely reported endogenous ligands for PPARα (*19*). We found most of the previously identified HETEs present in all crude brain tissue extracts (Fig. 2D). The previously identified PPARα ligands, HEX and OCT (*23*), were also present in crude brain extracts with high relative abundances, but like the other previously reported ligands, we only found these nonspecifically bound to beads and not enriched by PPARα (table S1 and fig. S2). Together, we attribute the selective PPARα binding of 7-HDHA to the stringency of our method and the inherent relative affinities and specificities of the various compounds.

7-HDHA exists in two isomeric forms, 7(*S*)-HDHA and 7(*R*)-HDHA. 7(*S*)-HDHA is produced from DHA by the enzyme Alox-5 (*39*). The previously demonstrated existence of both C-7 hydroxyl *R* and *S* isomers of known HDHA variants [7*R*,14*S*-diHDHA (maresin 1, MaR1); 7*S*,8*R*,17*S*-triHDHA (resolvin D1, RvD1); and 7*S*,16*R*,17*S*-triHDHA (resolvin D2, RvD2) (*40*, *41*)] suggests that both enantiomers, 7(*R*)- and 7(*S*)-HDHA (Fig. 2E), can be produced in vivo. Both enantiomers of 7-HDHA have previously been found in rat brains, but their relative distributions and abundances remain unclear (*42*). To investigate whether one enantiomer predominates and/or interacts

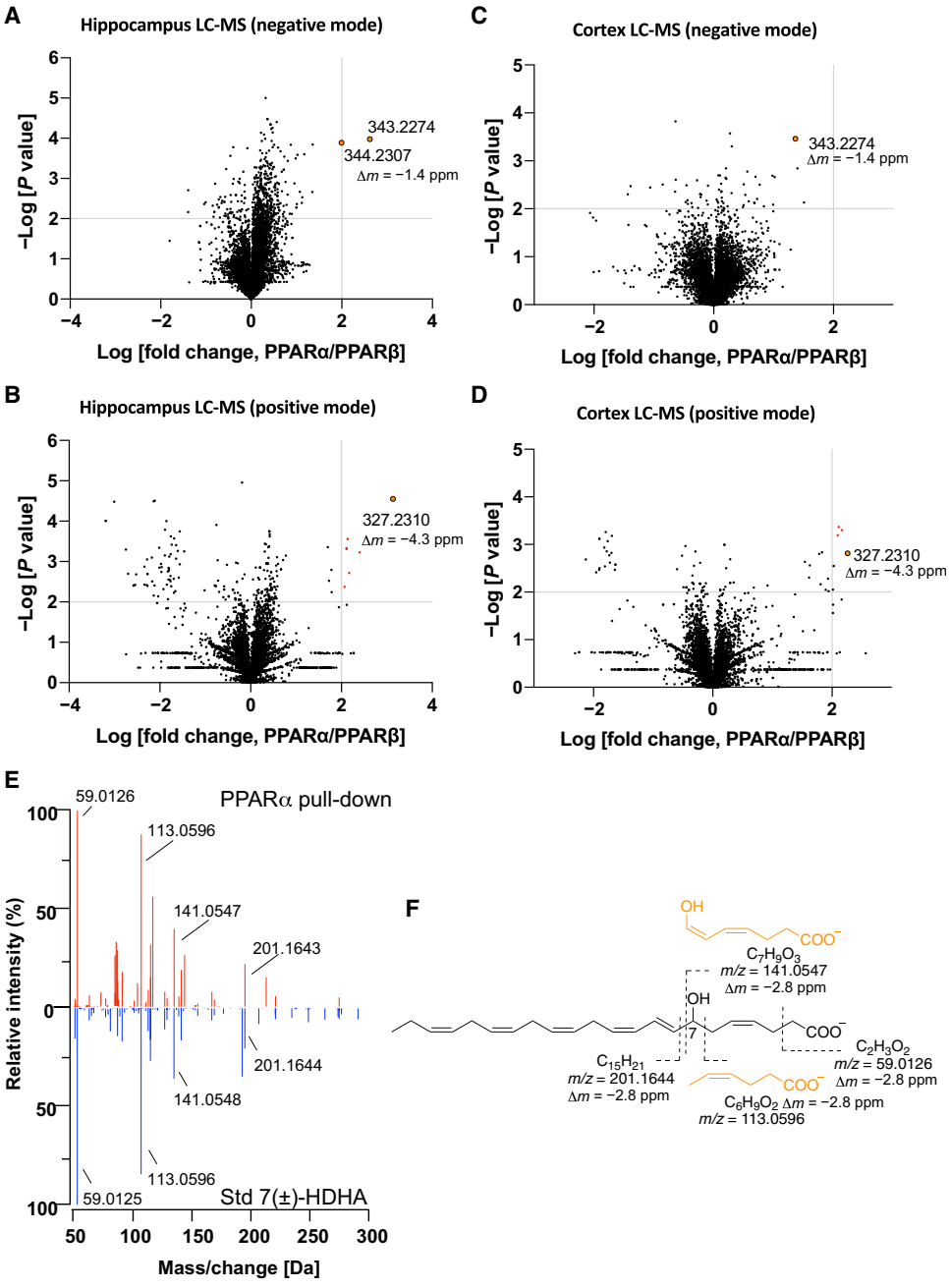

Fig. 1. The PPARα-LBD selectively enriches 7-HDHA from hippocampal and cortical lipidomes. (**A** to **D**) His-PPARα-LBD was incubated with a pool of lipids from the hippocampus (A and B) and cortex (C and D), and bound lipid extracts were analyzed by untargeted LC-MS in negative and positive modes (pull-downs were performed in triplicate, $n = 3$). Red dots indicate the ions with >100-fold enrichment and $P < 0.01$ in the PPARα sample. HDHA was the only extract-specific lipid that was strongly and consistently enriched by PPARα in both negative and positive modes. (**E** and **F**) Fragment ions and proposed structure of 7-HDHA identified by LC-MS^2 spectra in negative ion mode from *m/z* 343.2274, $\Delta m = -1.4$ ppm.

preferentially with PPARα, we synthesized 7-HDHA in racemic form (*43*) and then used a chiral high-performance liquid chromatography (HPLC) column to separate the two enantiomers. Their respective configurations were then elucidated using electronic circular dichroism (ECD). The ECD spectra exhibited a positive Cotton effect (CE) at around 240 nm and a negative CE at 220 nm (Fig. 2F) for the 7(*S*)-HDHA isoform, whereas the opposite CEs at 220 and 240 nm are consistent with the 7*R* configuration (*44*). Although both enantiomers were subsequently found to be present at similar levels in brain extracts, only one was pulled down by PPARα (Fig. 2G and fig. S3). By comparing their retention times with that of the standards, we determined that the copurified enantiomer is the 7(*S*)-HDHA isomer (Fig. 2G and fig. S3).

7(*S*)-HDHA interacts directly with PPARα

To assess and confirm the thermodynamics of 7-HDHA binding to PPARα, we first used isothermal titration calorimetry (ITC). Titration of a solution of the His-tagged PPARα-LBD using the mixed 7(±)-HDHA isoforms showed strong thermal stabilization with a binding dissociation constant (K_d) of ~1 μM, and a binding enthalpy (ΔH) of ~−6.5 kcal/mol (Fig. 3A). Similar testing of 4(±)- and 17(±)-HDHAs showed no effects on PPARα thermal stability (fig. S4, A and B). The 1 μM K_d obtained with the racemic mixture is consistent with the 0.5 μM value obtained using time-resolved fluorescence resonance energy transfer (TR-FRET) on the pure 7(*S*)-HDHA isoform (Fig. 3B). ITC testing also showed that 7(±)-HDHA had no effect on the thermal stability of the His-PPARβ-LBD (fig. S4C).

To further ascertain the nature of the physical interaction between 7(*S*)-HDHA and the PPARα LBD, several additional biophysical assays were used. First, in a cell-free, TR-FRET assay, competitive displacement of a prebound fluorescent ligand demonstrated that 7(*S*)-HDHA binds to the hPPARα-LBD with an IC_{50} of ~0.5 μM and a K_d of 0.2 μM (Fig. 3B). In contrast, the interaction of 7(*R*)-HDHA was about 10-fold lower, with an IC_{50} of ~5 μM and K_d of 1.8 μM (Fig. 3B). As with the *R* isoform, the previously reported PPARα ligands OA (*19*), stearic acid (SA), and OEA (*45*) also exhibited lower affinities in the micromolar range (fig. S5).

To query the potential reasons for the 10-fold selectivity of the 7(*S*)-HDHA over the 7(*R*)-HDHA isomer, we performed molecular docking using the application Glide (Schrödinger Inc.) and using a crystal structure of the PPARα LBD cocrystallized with eicosapentaenoic acid (EPA) and a seroid receptor coactivator 1 (SRC1) coactivator peptide as guide [Protein Data Bank (PDB) code 7BQ4; 1.62 Å]. As

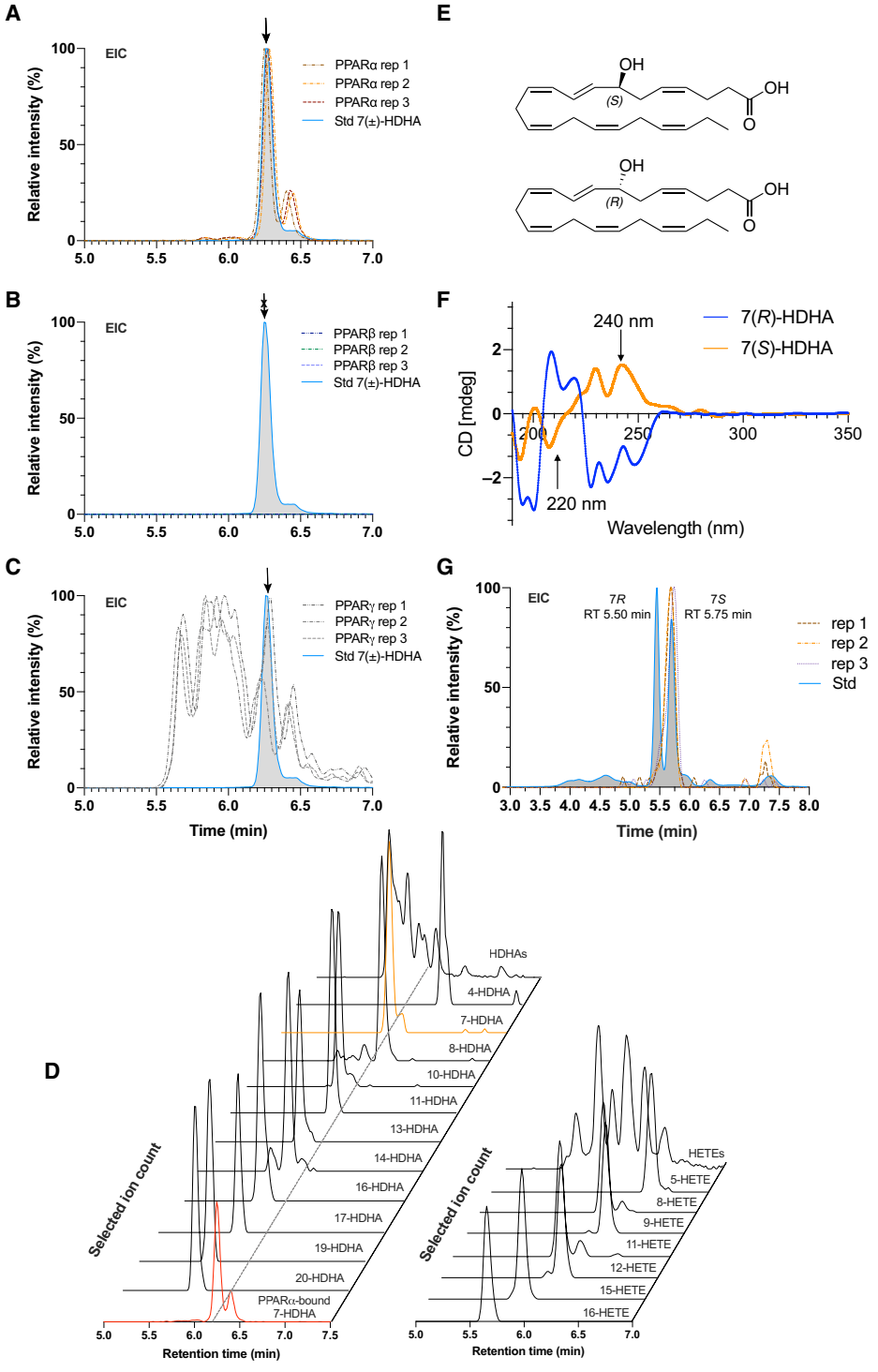

Fig. 2. The PPARα-LBD selectively binds 7(*S*)-HDHA. (**A** to **C**) Extracted-ion chromatograms (EICs) of HDHA (*m/z* 343.2274, Δ*m* = −1.4 ppm) pulled down by PPARα (A), PPARβ (B), and PPARγ (C). Shaded areas indicate the 7-HDHA standard (Std). Data were obtained from triplicates (reps 1 to 3) and compared with the standard. (**D**) EICs of fragment ions generated by parallel reaction monitoring (PRM) transitions (see table S2) for individual HDHA (*m/z* 343.2274, Δ*m* = −1.4 ppm, left) and HETE (*m/z* 319.2273, Δm = −0.1 ppm, right) isoforms detected in the hippocampal lipidomes. Red chromatograph indicates the 7-HDHA signal from the extracted PPARα pull-down. The last chromatogram in each series is the summation of EIC of HDHAs and HETEs. (**E**) Chemical diagrams of 7(*S*) and 7(*R*)-HDHAs indicating the chiral center at C7. (**F**) Experimental electronic circular dichroism spectra of synthesized 7(*R*)-HDHA and 7(*S*)-HDHA. (**G**) Comparison of 7-HDHA enantiomer chiral chromatograms of standard 7(±)-HDHA (Std) and PPARα pull-down from three experiments (rep 1 to 3).

has been shown for EPA and other fatty acid PPARα ligands (*23*, *46*), 7(*S*)-HDHA and 7(*R*)-HDHA, the LBD amino acids Ser^{280}, Tyr^{314}, His^{440}, and Tyr^{464} were predicted to form hydrogen bonds with the common -COOH moieties (Fig. 3C). The hydroxy group of 7(*S*)-HDHA was also predicted to form an additional H-bond with the sulfhydryl side chain of Cys^{276}, whereas the 7(*R*)-HDHA isoform was not (Fig. 3C). Comparison of 7(*S*)-HDHA docked in the PPARα LBD with the co-crystallized ligand EPA shows a very similar overlay, suggesting that both molecules occupy the same region of the PPARα ligand pocket, with the longer HDHA tail and Cys^{276} interaction being the exceptions (fig. S6).

To test the importance of the predicted Cys^{276} interaction, we mutated Cys^{276}, as well as the adjacent Cys^{275} residue, individually to alanine residues. Thermal shift assays were then performed to quantify the levels of thermal stabilization brought about by bound ligand. Wild-type and mutated hPPARα-LBDs all displayed comparable melting point curves in the absence of ligand (Fig. 3, D to F), confirming that the mutations did not introduce significant perturbations to hPPARα-LBD structure and thermal stability. As predicted, 7(*S*)-HDHA increased the PPARα LBD resistance to heat with a large melting temperature shift (ΔT_m) of 5.5°C (Fig. 3D), whereas 7(*R*)-HDHA had a much smaller effect (ΔT_m of 1.5°C; Fig. 3D). The melting temperature (T_m) shift for the wild-type hPPARα-LBD was also found to be ligand dose dependent (fig. S7). The C275A substitution actually led to a slight increase in thermal stability upon 7(*S*)-HDHA addition, with a melting temperature shift (ΔT_m) of 6.7°C (Fig. 3E). In contrast, substitution of the Cys^{276} residue with alanine did not change the thermal stability of the unliganded hPPARα-LBD but rendered the protein unresponsive to 7(*S*)-HDHA (Fig. 3F). These results are consistent with the predicted Cys^{276}–7(*S*)-HDHA hydrogen bond interaction, which increases ligand affinity and LBD conformational stability.

7-HDHA stimulates PPARα transcriptional activity

To determine whether 7(*S*)-HDHA has an impact on PPARα transcriptional activity, we performed a standard transient transfection assay using a fusion protein containing the DNA binding domain (DBD) of

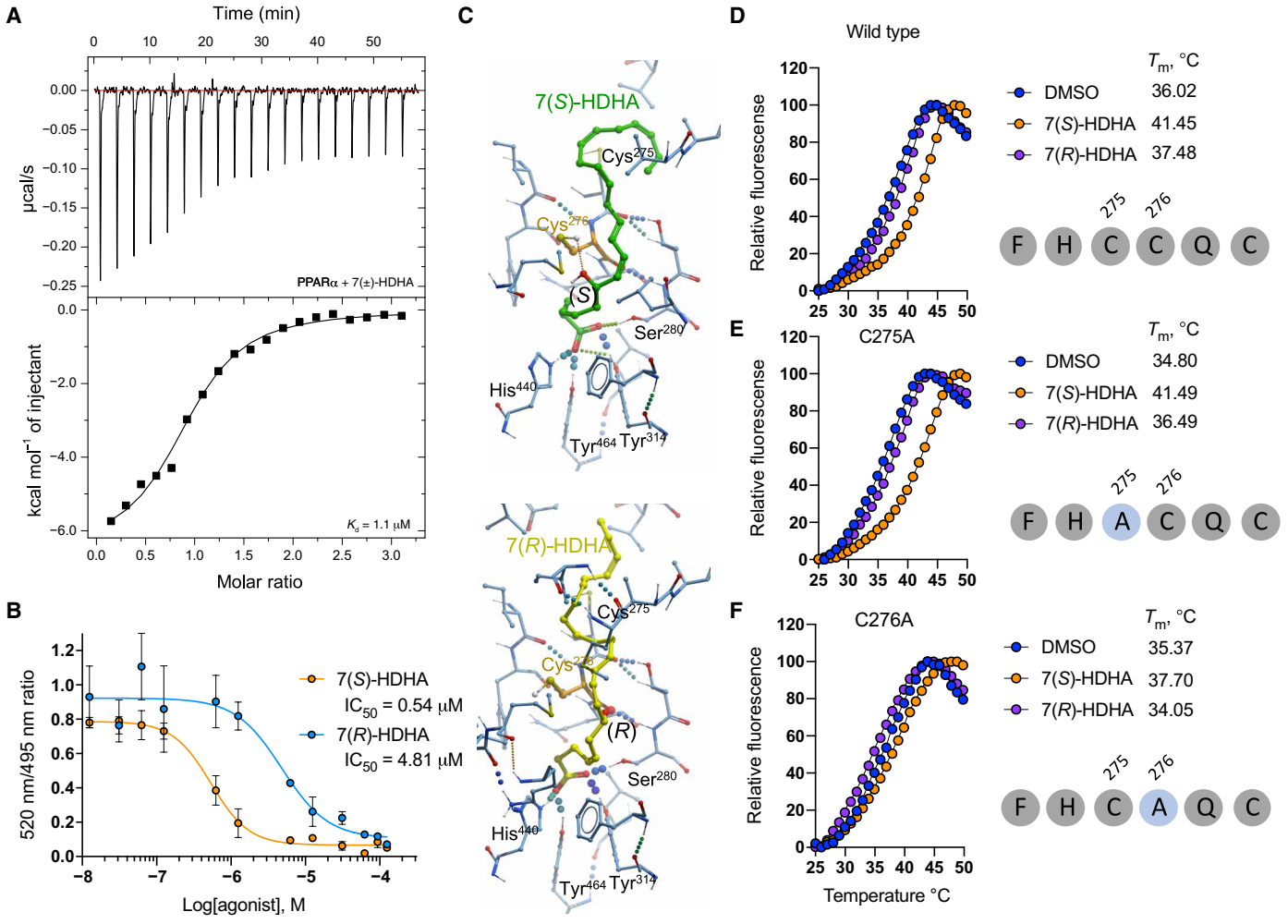

Fig. 3. Analyses of ligand interactions with PPARα. (**A**) Isothermal titration calorimetry (ITC) characterization of PPARα interaction with 7(±)-HDHA. Representative thermograms (upper row) and corresponding binding isotherms (lower row) are shown. (**B**) Comparison of binding affinities of 7(*S*)-HDHA and 7(*R*)-HDHA to the human PPARα-LBD using TR-FRET. Values derived are given for both IC_{50}s. The assay was validated using the full agonist GW7647 (see fig. S14). Data represent the means ± SEM from $n = 4$ experiments. (**C**) Docking of 7(*S*)- and 7(*R*)-HDHA in PPARα LBD (PDB code 7BQ4, 1.62 Å). Residues in proximity to the ligands are shown for clarity. The Cys^{276} side chain is shown in tangerine. (**D** to **F**) Thermal shift assays of WT-PPARα (D), C275A-PPARα (E), and C276A-PPARα (F) alone or with 7(*S*/*R*)-HDHAs, each performed in triplicate. Data are representative of $n = 3$ experiments. Tm represents the melting temperature.

yeast GAL4 attached to the hPPAR LBD, along with a UAS_{GAL4}-luciferase reporter, transfected together into cultured human embryonic kidney (HEK) 293 cells (*47*). We first compared the activities of 7(±)-HDHA on the three human PPAR gene LBDs. Consistent with our pull-down assay, 7(±)-HDHA strongly activated the PPARα fusion protein but had no significant effect on the PPARβ fusion protein (Fig. 4A and fig. S8A). Although 7(±)-HDHA was able to activate the PPARγ fusion protein, the levels required were significantly higher (EC_{50} = 44 µM versus 6 µM; Fig. 4A and fig. S8B). The 7(*S*)-HDHA isomer also had significantly stronger effects than the (*R*) isomer on reporter gene response levels (Fig. 4B and fig. S9). However, this difference was complicated by differential isomer stabilities and uptake by the HEK293 cells used in this assay, with the (*R*) isomer reaching much higher intracellular concentrations than the (*S*) isomer (fig. S10), making the calculated EC_{50}s for the *S*-isomer relatively high.

Next, we compared the activity of 7(±)-HDHA to other HDHAs and other previously identified PPAR ligands (Fig. 4C). Our results show that the majority have much higher EC_{50}s and much lower levels of transcriptional activation. The previously identified ligands 9(±)- and 13(±)-hydroxyoctadecadienoic acids (HODEs) (*48*) did exhibit comparable EC_{50}s with 7(±)-HDHA [6 and 3 µM, respectively, versus 6 µM; Fig. 4C and fig. S11), likely because the 9- and 13-hydroxyl groups can form the same additional C276 LBD contact as the 7-hydroxy of 7(*S*)-HDHA. These HODEs were not pulled down by PPARα from brain extracts, however, as they were not present at significant levels.

7(*S*)-HDHA promotes neuronal morphology through PPARα

Neuronal morphogenesis is critical for the proper formation of neuronal networks. During development, neuronal connections are established when axons and dendrites form synaptic contacts. Given

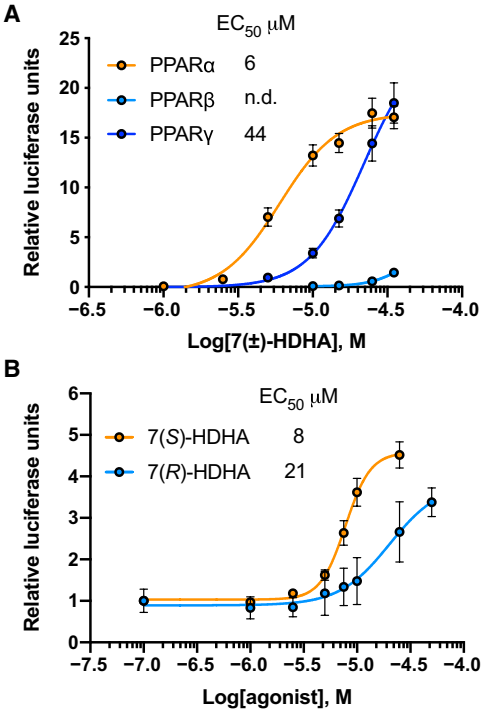

C

Tested metabolite	EC_{50} (μM)	Maximum activation % of GW7647
7(±)-HDHA	6	72.4 ± 9.7
13(±)-HODE	3	86.5 ± 3.1
9(±)-HODE	6	17.5 ± 0.9
4(±)-HDHA	15	35.1 ± 5.7
17(±)-HDHA	22	45.9 ± 1.8
OA	35	105.3 ± 16.8
SA	40	30.6 ± 1.5
OCT	n.d.	33.3 ± 1.1
HEX	n.d.	21.2 ± 6.0
OEA	n.d.	16.2 ± 1.5

Fig. 4. 7(*S*)-HDHA effects on PPARα transcriptional activity. (**A**) HEK293 cells were transfected with GAL4-hPPAR-LBDs and UAS luciferase constructs and then treated with 7(±)-HDHA for 16 hours. Absolute luciferase units were normalized to β-galactosidase activity and then multiplied by incubation time after addition of β-galactosidase buffer. Data are expressed as means ± SD ($n = 3$). n.d., not determined. Representative curves of three independent experiments are shown. (**B**) HEK293 cells were transfected with GAL4-hPPARα-LBDs and UAS luciferase constructs and then incubated with 7(*R*)-HDHA or 7(*S*)-HDHA enantiomers for 5 hours. Data shown are the mean luciferase values obtained from triplicate wells normalized by β-galactosidase activity. Data represent the means ± SD ($n = 3$). Representative curves of three independent experiments are shown. (**C**) Summary of activation effects of 7(±)-HDHA as compared to previously identified PPARα endogenous ligands. The EC_{50} of OEA could not be determined because of extremely low solubility. HEX and OCT displayed substantial cytotoxicity with higher concentrations (*23*); thus, their EC_{50}s could also not be determined. Data shown are the mean luciferase values obtained from triplicates and normalized to β-galactosidase activity. EC_{50}s represent the mean, and maximum activation values are expressed as means ± SD ($n = 3$).

that PPARα has been shown to be present and functional in the brain (*8*–*10*) and that DHA has been shown to regulate various neuronal developmental processes including neuronal differentiation (*49*), dendritic arborization (*50*), and spinogenesis (*51*), we investigated the potential role of 7(*S*)-HDHA in primary embryonic mouse cortical neurons. Isolated neurons were initially treated with 7(*S*)-HDHA at concentrations from 0.1 to 1 μM. Because lethality was noted at concentrations of 0.75 μM and above, and no differences in response were observed between 0.1 and 0.5 μM, all subsequent treatments were at 0.1 μM, which is in the range of normal 7-HDHA concentrations in the brain (*36*). Notably, our analyses showed that 7(±)-HDHA concentrations in rat cortex were ~0.5 nmol/g [~0.5 μM assuming 1 g of brain tissue is ~1 ml; (*52*)] in the absence of DHA supplementation and ~1 nmol/g (~1 μM) with DHA supplementation (fig. S12), with the *S* and *R* isoforms present at roughly equal levels.

Cortical neurons treated with 0.1 μM 7(*S*)-HDHA displayed an increase in both the number of dendrites per neuron (Fig. 5, A and B, and fig. S13) and in overall neurite (Fig. 5C) and dendrite length (Fig. 5D). The length of the longest neurite (the prospective axon) was not altered (Fig. 5E), indicating that 7(*S*)-HDHA acts predominately on dendrites. These responses to 7(*S*)-HDHA were similar to those induced by the synthetic PPARα agonist GW7647 used at a 10-fold higher concentration (1 μM).

Next, we assessed the requirement for PPARα in this dendritic response by attenuating PPARα expression using small interfering RNAs (siRNAs). The expression of PPARα in cortical neurons was reduced by ~70% after siRNA treatment (Fig. 5F), demonstrating the effective knockdown of PPARα. In PPARα knockdown neurons treated with 7(*S*)-HDHA, the increase in the number and overall length of dendrites was lost (Fig. 5, A to D). Thus, PPARα is required for the 7(*S*)-HDHA–induced change in dendritic morphology. Treatment with the PPARα antagonist GW6471 (1 μM) reduced total neurite length (Fig. 5C), but when broken down into effects on dendrites and prospective axons, the effect was isolated to axons (Fig. 5E). Given that the knockdown of PPARα had no significant effect on either dendrite or axon length, we suspect the simplest explanation for the antagonist effect on axons is that it is an off-target effect. In this regard, we note that GW6471 has recently been reported to be a potent antagonist of both PPARα and PPARγ (*53*).

Previous work identified a panel of PPARα-regulated genes that act to modulate neuronal plasticity (*13*). Thus, we next explored the effect of 7(*S*)-HDHA in primary cortical neurons on the expression of several of these, including *Creb* and the genes expressing two subunits of the multimeric glutamate receptors, α-amino-3-hydroxy5-methyl-4-isoxazolepropionic acid receptor (AMPAR) and *N*-methyl-*D*-aspartate receptor (NMDAR), all of which are known to be vital for synaptic plasticity (*54*–*56*). Our analysis revealed that 7(*S*)-HDHA specifically promotes the expression of *Creb* and *GluR1* (AMPAR subunit), but not *Nr2b* (the NMDAR subunit) (Fig. 5G). Consistently, knockdown of PPARα resulted in loss of 7(*S*)-HDHA–induced expression of *Creb* and *GluR1*. Together, these results indicate that 7(*S*)-HDHA induces the expression of genes important for neuronal plasticity in a manner that requires PPARα.

DISCUSSION

In conclusion, we found that the omega-3 hydroxy fatty acid 7(*S*)-HDHA is a high-affinity, natural PPARα transcriptional activator, with potent activity in the mouse brain. What appears to be key to

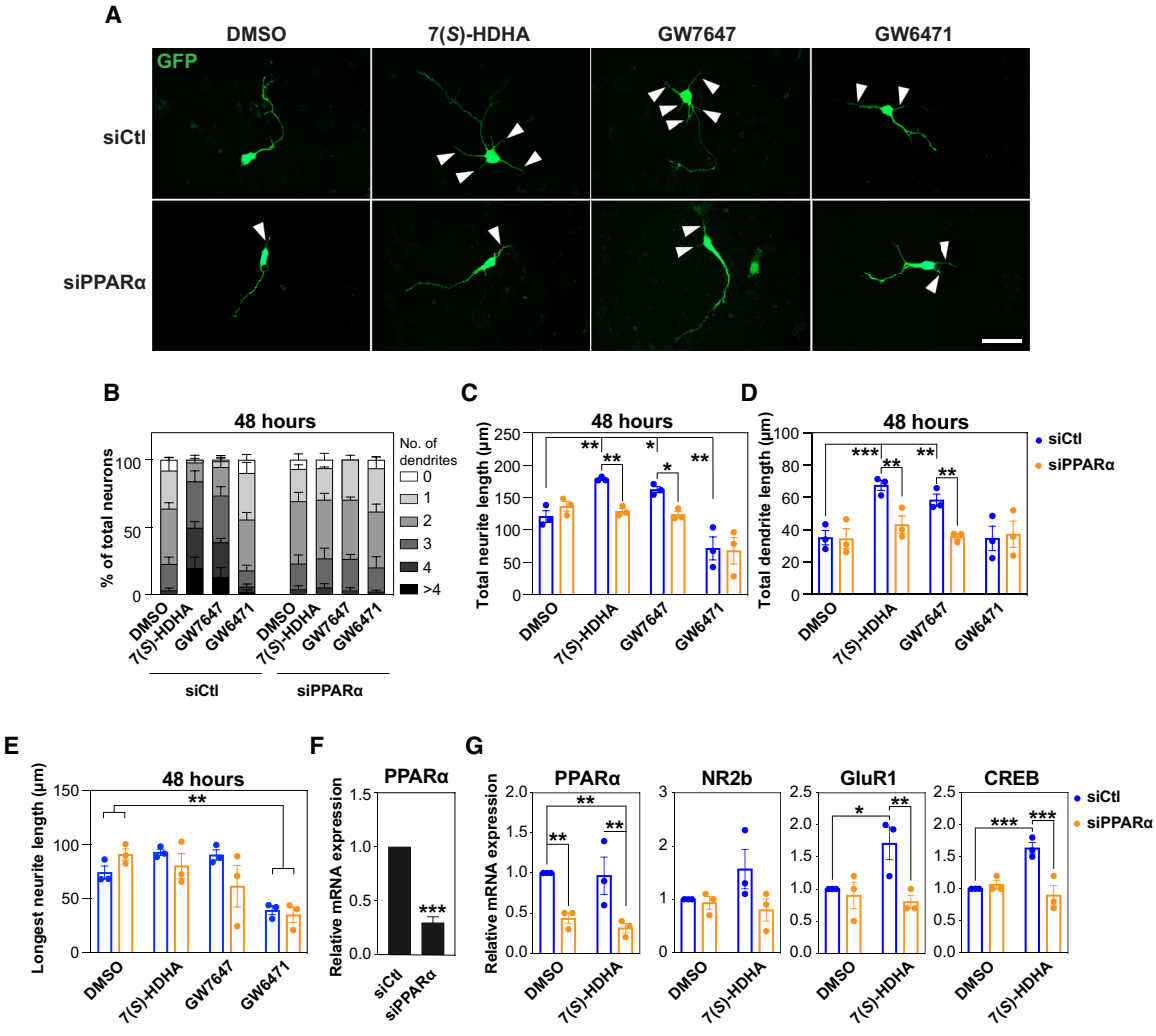

Fig. 5. 7(*S*)-HDHA effects on dendrite formation. (**A**) Dissociated E15.5 to E16.5 mouse cortical neurons were electroporated with siRNA against PPARα (siPPARα) or siControl (siCtl) along with eGFP and then treated with 7(*S*)-HDHA (0.1 μM), GW7647 (1 μM), or GW6471 (1 μM) 4 hours after plating. Neurons were fixed at 48 hours, and neuronal morphology was examined in GFP-positive neurons. Representative images are shown. Scale bar, 50 μm. (**B**) Quantification of the number of dendrites (neurites with length <5 × the somal diameter) from a minimum of 90 neurons from $n = 3$ independent experiments as a percentage of total neurons is plotted as the means ± SEM. (**C** to **E**) Quantification of the total length of all neurites (axons and dendrites; C), all dendrites (longest neurite excluded; D), and longest neurite (prospective axon, E) is plotted as the means ± SEM from $n = 3$ independent experiments. Each dot represents the median length of minimum $n = 30$ neurons from one of the three independent experiments. (**F**) PPARα siRNA knockdown efficiency for (A) to (C). RNA was isolated from GFP-positive neurons after FACS. Relative mRNA expression is plotted as means ± SEM from $n = 3$ independent experiments. (**G**) Assessing the requirements of PPARα for 7(*S*)-HDHA–induced gene expression. Cortical neurons were electroporated with siPPARα or siControl along with eGFP, plated for 24 hours, and then treated for 6 hours with 7(*S*)-HDHA. Gene expression was measured by qPCR in GFP-positive neurons and is plotted as means ± SEM from $n = 3$ independent experiments. Statistical significance: $^{*}P < 0.05$, $^{**}P < 0.01$, and $^{***}P < 0.001$, using either two-tailed unpaired *t* test for two groups or two-way ANOVA with two-stage linear step-up procedure of Benjamini, Krueger, and Yekutieli for multiple comparisons.

this specificity, affinity, and full agonist activity is the ability of the C7 hydroxyl group of 7(*S*)-HDHA to form a hydrogen bond with Cys^{276} on helix-3 of the PPARα LBD. Activation of PPARα in primary cortical neurons peaked at a physiologically relevant concentration of ~0.1 μM, resulting in the activation of PPARα target genes known to be involved in neuronal plasticity, culminating in increased dendrite numbers and lengths.

Whether 7(*S*)-HDHA, like DHA, crosses the blood/brain barrier remains unclear. Given their similarities, the carrier or transporter responsible for DHA transportation into the brain could also do the same for 7(*S*)-HDHA. In terms of de novo production in the brain, 7(*S*)-HDHA would most likely be produced from DHA by the enzyme Alox-5, which upon lipid binding has been shown to translocate to the nuclear envelope where it interacts with 5-lipoxygenase activating protein (FLAP), a protein that activates Alox-5 enzymatic activity (*57*). As with prostaglandins and leukotriene A4, 7(*S*)-HDHA is then likely transported within the nucleus by fatty acid–binding proteins (FABPs) (*58*). Lipid-bearing FABPs have also been shown to interact with PPARγ at PPAR response elements, with direct transfer of their lipid ligands and subsequent PPAR target gene activation (*59*). This type of directed subcellular concentration enrichment may also explain how other PPAR lipid ligands are able to activate their receptors at concentrations below reported LBD K_ds or EC_{50}s measured in vitro or in cultured cell experiments (*60*).

Regulated in vivo LBD posttranslational modifications could also play a role in ligand binding and responses.

Together, our findings suggest that maintaining or boosting 7(*S*)-HDHA levels in the brain may have potential as a specific and safe strategy for the prevention and treatment of cognitive and neurodegenerative diseases. Potential roles for 7(*S*)-HDHA in the treatment or prevention of other PPARα- and ω-3 FA–related disorders should also be investigated.

MATERIALS AND METHODS

Animal experiments

All experimental procedures were conducted in accordance with the guidelines of the Canadian Council on Animal Care and approved by the University Animal Care Committee and Research Oversight and Compliance Office of University of Toronto, Canada. For brain lipid extraction, 2-week-old C57BL/6J male/female pups were housed (8 to 10 mice per cage) on a 12-hour light/12-hour dark cycle with food and water provided ad libitum.

For primary neuron cultures, CD1 timed-pregnant female mice were purchased from Charles River Laboratories and housed on a 12-hour light/12-hour dark cycle with food and water provided ad libitum.

For measurement of 7(±)-HDHA in rat cortex, two Long Evans dams, each with eight 18-day-old male nonlittermate Long Evans pups, were ordered from Charles River Laboratories (St. Constant, QC, Canada). After arrival at the University of Toronto, the dam and pups were acclimated for 3 days on 2% α-linolenic acid (ALA) in total fat diet and then weaned at 21 days old. At weaning, the 21-day-old pups were placed on a 10% by weight fat diet containing either 2% ALA in total fatty acids or 2% DHA + 2% ALA in total fatty acids as the only dietary ω-3 fatty acids for 8 weeks until 11 weeks of age. Brains were collected from rats after anesthesia with 5% isoflurane to effect and maintained at 3% isoflurane and subsequent euthanasia by excision of the heart. (*61*).

Reagents

Standard 7(±)-HDHA (33300), 4(±)-HDHA (33200), 17(±)-HDHA (33650), 9(±)-HODE (38400), 13(±)-HODE (38600), GW7647 (10008613), GW501516 (10004272), rosiglitazone (71740), SR1078 (16503), fexaramine (17369), HEX (21086), OCT (90375), OEA (90265), OA (90260), SA (10011298), EPA (90110), DHA (90310), and AA (90010) were purchased from Cayman Chemical. LA (L1376) and 1-palmitoyl-2-oleoyl-sn-glycero-3-phosphocholine (850457P) were purchased from Sigma-Aldrich.

Metabolome isolation

Cerebral cortex, cerebellum, and hippocampus tissues of 2-week-old C57BL/6J mice were homogenized in five volumes of ice-cold phosphate-buffered saline (PBS) solution (10 mM, pH 7.4) for 2 min. Lipids were extracted from tissues using the modified Bligh and Dyer method (*62*). Ice-cold methanol (500 μl) containing 100 μM butylated hydroxytoluene (BHT) was added to each sample (500 μl of brain homogenate). The mixtures were incubated for 30 min in the dark at 37°C, then cooled on ice, and extracted with 1 ml of chloroform/methanol/water (4:5:1, v/v/v). Samples were then mixed with a vortex mixer for 1 min and centrifuged at 1500*g* for 5 min at 4°C. The chloroform/methanol layer was dried with nitrogen, and the residue resuspended in 100 μl of dimethyl sulfoxide (DMSO). The method of quantification of endogenous 7-HDHA was reported previously (*63*). A total of 100 mg of rat cortex previously frozen at −80°C was defrosted from on ice. After the tissue was weighed, internal standard (50 μl) and 1 ml of ice-cold MeOH (for brain tissue ≤100 mg ≈ 10% of final volume) were added and then homogenized. Samples were kept at −20°C for 45 min to allow protein precipitation and centrifuged at 12,000*g* for 10 min (4°C). The supernatant was then applied on a preequilibrated C18 cartridge (Hypersep Silica 500 mg, 60108-411, Thermo Fisher Scientific). Thirty seconds before loading samples, 9 ml of H_2O (pH 3.5) was added to rapidly acidify and bring sample to <10% of the total volume. After confirming acidification of the sample to a pH of 3.5 with pH strip and adjustment with two to four drops of 2 M HCl, the samples were loaded onto the cartridge. Ten milliliters of hexane (dropwise) was passed through each cartridge, stopping the flow just before the meniscus reaches the sorbent bed. The tubes under each cartridge (borosilicate glass) were changed before elution with 8 ml of methyl formate (dropwise). The tubes with samples were placed on ice and stored away from light. After drying the samples with nitrogen, they were resuspended in 100 μl of MeOH.

Pull-downs

Human PPARα (residues 192 to 468), PPARβ (residues 169 to 440), PPARγ (residues 206 to 471), ERRγ (residues 229 to 457), NOR1 (residues 394 to 626), NURR1 (residues 353 to 598), RORγ (residues 261 to 507), and FXR (residues 217 to 472) LBDs were expressed in *Escherichia coli* BL21 (DE3) cells as TEV-cleavable 6× histidine-tagged fusion proteins. Cultures were grown in Terrific Broth medium at 37°C until an OD_{600} (optical density at 600 nm) of 1.0 was reached. The temperature was then decreased to 17°C, and cultures were induced with 0.1 mM isopropyl 1-thio-β-D-glucopyranoside for 16 hours. Harvested bacterial pellets were resuspended in buffer containing 20 mM tris/HCl (pH 8.2), 300 mM NaCl, 5 mM imidazole, and 0.5 mM dithiothreitol (DTT). After sonication of the cells (5 min at 40% amplitude using cycles of 10 s on/10 s off) and centrifugation at 18,000*g* at 4°C for 20 min, supernatants were incubated with mouse lipidome samples (1:100, v:v) and 7 μl of HIS-select nickel magnetic agarose beads (H9914, Sigma-Aldrich) for 1 hour at 4°C and then for 30 min at room temperature. Flowthroughs were removed using a magnetic stand. After washing three times with 100 μl of buffer containing 20 mM tris/HCl (pH 8.2), 300 mM NaCl, and 30 mM imidazole, the His-tagged LBD-ligand complexes were eluted with 50 μl of buffer containing 20 mM tris/HCl (pH 8.2), 300 mM NaCl, and 300 mM imidazole using a magnetic stand.

LC-MS analysis

Elution samples were loaded onto a Zeba spin desalting plate [7K MWCO (89807), Thermo Fisher Scientific] and then centrifuged at 1500*g* at 4°C for 2 min. The desalted samples were then evaporated by SpeedVac and resuspended in HPLC grade methanol. LC-MS was performed using a Thermo Fisher Scientific Q Exactive HF Hybrid Quadrupole-Orbitrap mass spectrometer. Samples were first loaded onto a reverse-phase column (Accucore Vanquish C18+ 50 × 2.1 mm, Thermo Fisher Scientific) using the ultra performance liquid chromatography (UPLC) System in methanol and eluted with a gradient of 90% mobile phase A (H_2O containing 0.1% formic acid) and 10% mobile phase B (methanol containing 0.1% formic acid), at time 0, with a flow rate of 0.15 ml/min, increasing to 80% mobile phase B at 2 min, 85% mobile phase B at 7 min, and then 100%

mobile phase B at 8 min and kept isocratic for 0.5 min, before returning to 90% mobile phase A over the next 1.5 min. The temperatures of the column and sample compartments were maintained at 40° and 10°C, respectively. Data were acquired in full MS and parallel reaction monitoring (PRM) mode. Parameters for full MS scan were recorded at resolution R = 70,000 with a maximum of 3×10^6 ions collected within 200 ms, followed by PRM MS/MS scan recorded at resolution R = 17,500 (at m/z 343.2274) with a maximum of 3×10^6 ions collected within 200 ms. Chiral LC-MS/MS was performed with a chiral column (see below) using a gradient of 80% mobile phase B, at time 0, with a flow rate of 1 ml/min, increasing to 90% mobile phase B at 2 min, then increasing to 100% mobile phase B at 7 min, kept isocratic for 1 min, and then returned to 80% mobile phase B over the next 0.5 min.

Untargeted metabolomics data analysis was performed using an in-house R program. Specifically, raw MS files were converted to open format (.mzXML). Chemical features were detected with XCMS package at 2.5-ppm mass accuracy. Features were matched across different samples with a 0.5-min retention time tolerance window. Putative metabolite features were selected by calculating the fold change of features from treatments relative to controls. Specifically, only those features with 100-fold higher abundances ($P < 0.01$) in PPAR LBDs over controls were considered as metabolite features.

PPAR recombinant protein production

Recombinant proteins were expressed as described above in the pull-down section. Proteins were purified using Ni^{2+}-NTA affinity Agarose (45 to 165 μm; Qiagen 30210) followed by size exclusion fast protein liquid chromatography (FPLC) (HiLoad 16/60 Superdex 200, GE Healthcare, Life Sciences) equilibrated with 150 mM NaCl, 50 mM HEPES (pH 8.2), and 0.5 mM DTT, at a flow rate of 1 ml/min.

Synthesis and purification of 7-HDHA enantiomers

A detailed description of 7(*S*)-HDHA synthesis has been published separately (*43*). The racemic mixture of synthetic 7(±)-HDHA was separated on a Chiralpak-IA column (amylose tris 3,5-dimethylphenylcarbamate, 250 × 4.6 mm; Chiral Technologies Europe) and eluted with an isocratic elution of 45% mobile phase A (H_2O containing 0.1% formic acid) and 55% mobile phase B (acetonitrile containing 0.1% formic acid). The temperatures of the column and sample compartments were maintained at 20° and 4°C, respectively. Data were acquired at a wavelength of 230 nm using a diode-array detection (DAD) detector.

Circular dichroism measurements

Circular dichroism (CD) spectra of the proteins were acquired on a Jasco J-1500 CD spectrometer at room temperature. Separated racemic 7-HDHA enantiomers were dissolved in HPLC grade methanol.

LanthaScreen TR-FRET PPARα competitive binding assays

The LanthaScreen TR-FRET PPARα competitive binding assay was performed according to the manufacturer's instructions (Invitrogen). Test compounds were incubated for 3 hours at room temperature with glutathione *S*-transferase (GST)–hPPARα–LBD (5 nM), LanthaScreen terbium-labeled anti-GST antibody (5 nM), and Fluormone pan-PPAR green (20 nM). The TR-FRET emission was measured with a Tecan Infinite F200 Fluorescence Microplate Reader. Results were expressed as the ratio of fluorescence intensity at 520 nm (fluorescein emission excited by terbium emissions) and 495 nm (terbium emissions). K_ds for the competitors were calculated by applying the equation: $Ki = IC_{50}/(1 + ([\text{competitor}]/K_d))$, where IC_{50} is the concentration of competitor that produces 50% displacement of the tracer. [tracer] is the concentration of Fluormone Pan-PPAR Green used in the assay (20 nM), and K_d is the binding constant of Fluormone Pan-PPAR Green to PPARα-LBD (12 ± 2 nM).

Site-directed mutagenesis of hPPARα-LBD

To generate point mutations in the ligand-binding pocket of hPPARα-LBD, the plasmid pET28-MHL-hPPARα-LBD was used as template for site-directed mutagenesis. Mutagenic substitutions were performed using In-Fusion Cloning technology (Takara). The primers included 15–base pair (bp) overlaps with each other at their 5′ ends highlighted in gray. Oligonucleotides (Eurofins) for the method were designed as shown in table S3.

Thermal shift assays

The thermostabilities of hPPARα-LBD in the presence of 7(*S*)-HDHA and 7(*R*)-HDHA were assayed using a Thermofluor-type assay. Briefly, 2 μl of 30 μM purified wild-type hPPARα-LBD, hPPARα-LBD C275A, or C276A mutants was dispensed into 96-well plates (~3 μM protein per well). Compounds in 100% (v/v) DMSO were serial diluted with DMSO and added into wells [1 μl for each reaction; final concentration of DMSO 1% (v/v)]. Fifteen microliters of thermal shift assay buffer was added into wells to make 18 μl of reaction solutions. Proteins and ligands were then incubated at 4°C for 2 hours. A 2 μl of aliquot of 100-fold SYPRO Orange dye (Sigma-Aldrich) was added into each well, and then wells were sealed. Dye and protein solutions were mixed by gently rotating for 15 s and spun down at 1000*g* for 1 min. Protein melting curves were measured using the QuantStudio 6 Flex Real-Time PCR System (Thermo Fisher Scientific) with the following program: 2 min at 25°C, ramp to 95°C at $1°C \cdot s^{-1}$, 2 min at 95°C, and excitation and emission wavelengths at 483 and 568 nm, respectively. The melting temperatures (T_ms) of the hPPARα-LBD wild-type and mutated proteins in the absence of ligands provided the baseline T_m (T_m0) for each protein. The thermo-shift effects of compounds presented in this study were obtained by plotting mean ΔT_ms ($T_m$ligand – T_m0) versus ligand concentration using data from at least three replicate experiments, as listed in Fig. 3 (D to F) and fig. S7. A three-parameter dose-response nonlinear repression function was fit to the data using the GraphPad Prism v5.04 (GraphPad Software, La Jolla, CA). The resultant curves, calculated EC_{50} values, and maximum T_m shifts for each compound are listed in fig. S7.

Isothermal titration calorimetry

Purified protein (25 μM) was dissolved in 400 μl of 150 mM NaCl and 20 mM HEPES (pH 7.5), and then equilibrated at room temperature for 1 hour before ITC measurement. All experiments were performed in an Auto-iTC200 calorimeter (Malvern Instruments) at 25°C. Ligands were used at a concentration of 200 μM. Two-microliter aliquots were added automatically to the PPAR LBDs in the calorimeter cell. Blank experiments (injections of ligand into buffer) were performed, and heat responses were subtracted. Control experiments performed by injection of the buffer to the protein solution yielded insignificant heats of dilution. Integrated heat effects were analyzed using Microcal Origin 7 software (Malvern Instruments).

Cell culture reporter assays

HEK293 cells were maintained in Dulbecco's modified Eagle's medium (DMEM) (Invitrogen, Carlsbad, CA) containing 10% fetal bovine serum (FBS) and 1× penicillin/streptomycin (P/S) at 37°C in a humidified atmosphere of 5% CO_2. For transfection assays, HEK293 cells were cultured into a clear-bottom white 96-well plate in DMEM supplemented with 10% charcoal-dextran stripped FBS (Gemini Bio-Products, Sacramento, CA). After overnight incubation, cells were transfected with the plasmid DNA using a calcium phosphate method. The plasmid DNA contained 50 ng of UAS-luciferase reporter, 15 ng of GAL4-hPPAR, 20 ng of β-galactosidase, and 65 ng of pGEM filler vector. Six hours after transfection, cells were treated with vehicle (DMSO) or various concentrations of compounds. The following day (16 hours after ligand addition), luciferase and β-galactosidase activities were determined. For experiments in which the ligand was added for only 5 hours, the HEK293 cells were transfected as described above but left overnight for 24 hours before addition of ligand. Five hours later, luciferase and β-galactosidase activity were determined. Luciferase values were normalized to β-galactosidase to control for transfection efficacy, and the results were expressed as relative luciferase units. Data were averaged from triplicate wells and presented as means ± SD.

Cell lysate preparation for quantification of 7(*R*/*S*)-HDHA levels

HEK293 cells were cultured at 4×10^5 cells per well in six-well plates using DMEM with 10% FBS and 1× P/S and maintained at 37°C and 5% CO_2. The next day, ligands were prepared in DMEM containing 10% charcoal-dextran stripped FBS, and cells were incubated with 25 μM 7(*R*)-HDHA or 7(*S*)-HDHA for 0, 0.5, 1, 2, 4, 7, or 16 hours. For each time point, medium was collected, and cells were harvested in 100 μl of PBS after washing two times with PBS. Cell and media samples were frozen at −20°C until extraction. Cell lysate samples were prepared using the solvent extraction approach described in the lipidome preparation section. Cell extracts were centrifuged, and the supernatants were withdrawn followed by drying. The dried samples were dissolved in 60 μl of methanol and then analyzed using a Thermo Fisher Scientific Q Exactive HF Hybrid Quadrupole-Orbitrap Mass Spectrometer.

Primary cortical neuron electroporation, culturing, immunofluorescence microscopy, and qPCR

Primary cortical neurons were isolated from embryonic day 15.5 (E15.5) to 16.5 CD1 mouse embryos. Dissociated neurons (4×10^6 to 5×10^6 cells) were electroporated with enhanced green fluorescent protein (eGFP) plasmid (2 μg) and/or siRNAs using the Amaxa mouse Nucleofector kit (Lonza) according to the manufacturer's protocol. Cells were then plated in chamber slides (Lab-Tek II) coated with poly-L-lysine (20 μg/ml; Sigma-Aldrich, P1399) and laminin (2 μg/ml; Corning, 354232). Neurons were cultured at 37°C and 5% CO_2 in Neurobasal medium (Gibco, 21103-049) supplemented with 2% B-27 (Gibco, 17504-044), 0.5% N-2 (Gibco, 17502-048), 2 mM GlutaMAX (Gibco, 35050-061), and 0.5% penicillin/streptomycin (Gibco, 15140-122). For immunofluorescence analysis, 7(*S*)-HDHA (100 nM) was added 4 hours after plating. Cells were fixed at 48 hours with 4% paraformaldehyde, washed three times for 5 min with PBS, and imaged for GFP fluorescence using the 40× Plan-NEOFLUAR objective of Zeiss Axiovert 200 M epifluorescence microscope. Images were taken randomly, and neurite length for a minimum 30 neurons per condition was quantified using Volocity software. For gene expression analysis, 7(*S*)-HDHA (100 nM) was added to electroporated neurons at 4 or 24 hours after plating for 48 or 6 hours, respectively, as indicated. Cells were trypsinized, and GFP-positive cells were isolated by FACS sorting. Total RNA was extracted using the Norgen Single-Cell RNA Purification Kit (catalog no. 51800), and complementary DNA was synthesized using 70 to 200 ng of purified RNA using oligo-dT primers and M-MLV Reverse Transcriptase. Real-time qPCR was performed using SYBR Green Master Mix (Applied Biosciences) on the QuantStudio 6 Flex System (Applied Biosciences). Relative gene expression was quantified using the $\Delta\Delta C_t$ method and normalized to glyceraldehyde-3-phosphate dehydrogenase (GAPDH). The primer sequences are listed in table S4.

Molecular modeling of 7-HDHA analogs

Docking of 7(*S*)- and 7(*R*)-HDHA in PPARα LBD structure (PDB code 7BQ4, 1.62 Å, cocrystallized with EPA and SRC1 coactivator peptide) was done using the Schrödinger Drug Discovery suite 2020-3 using Glide SP scoring v.5.0 (www.schrodinger.com/glide). The protein was prepared using the Protein Prep procedure using EPA to define the binding site. Keeping in mind the nearly linear shape of fatty acids, the inner docking box was elongated by 5 Å in two directions, resulting in the 10 Å by 15 Å by 15 Å inner box size. Missing side chains were filled in using PRIME, structural water orientations were sampled, protonation states of ionizable side chains were assigned with PropKa to pH 7, and only hydrogens were minimized using OPLS3. Three key H-bonds were set up as restraints (side chains of Ser^{280}, Tyr^{314}, and His^{440}) to anchor the acidic group and prevent it from bonding elsewhere. Hydroxyls of Cys^{275}, Cys^{276}, and Thr^{279} were treated as rotatable during the docking. The fatty acids were prepared for docking using LIGPREP. The ligands were ionized to pH 7 ± 2 and energy minimized using OPLS3. The docking was done using Glide SP scoring. Ten docking poses were saved out of 500 that were chosen for the postdocking minimization. The docking poses were ranked by emodel score and compared by Glide SP score.

The docking was validated first by redocking the EPA molecule back into the PPARα LBD, which provided excellent overlay against the cocrystallized form of EPA. Note that several 7(*S*)-HDHA docking poses contained an additional H-bond between the 7(*S*)-hydroxyl and side chain of Cys^{276}, whereas none of the 7(*R*)-HDHA docking poses were able to engage any additional H-bonds that involved the 7(*R*)-hydroxyl. The Glide SP docking scores were −10.52 and −9.75 for 7(*S*)-HDHA and 7(*R*)-HDHA, whereas the Glide emodel scores were −71.59 and −58.67 for the same stereoisomers, correspondingly.

Statistical analyses

The values in the luciferase reporter assay are expressed as the means ± SD. Differences among means were analyzed using one-way analysis of variance (ANOVA). The data in the neuronal image analyses are presented as means ± SEM and were analyzed by two-tailed unpaired *t* test for two groups or two-way ANOVA with two-stage linear step-up procedure of Benjamini, Krueger, and Yekutieli for multiple comparisons in GraphPad PRISM (GraphPad Software Inc., La Jolla, CA). $P < 0.05$ was considered significant (*$P < 0.05$, **$P < 0.01$, and ***$P < 0.001$).

SUPPLEMENTARY MATERIALS

www.science.org/doi/10.1126/scisignal.abo1857
Figs. S1 to S14
Tables S1 to S4
Reference (*64*)

View/request a protocol for this paper from *Bio-protocol*.

REFERENCES AND NOTES

1. M. A. Lazar, Maturing of the nuclear receptor family. *J. Clin. Invest.* **127**, 1123–1125 (2017).
2. R. M. Evans, D. J. Mangelsdorf, Nuclear receptors, RXR, and the big bang. *Cell* **157**, 255–266 (2014).
3. M. Uhlen, L. Fagerberg, B. M. Hallstrom, C. Lindskog, P. Oksvold, A. Mardinoglu, A. Sivertsson, C. Kampf, E. Sjostedt, A. Asplund, I. Olsson, K. Edlund, E. Lundberg, S. Navani, C. A. Szigyarto, J. Odeberg, D. Djureinovic, J. O. Takanen, S. Hober, T. Alm, P. H. Edqvist, H. Berling, H. Tegel, J. Mulder, J. Rockberg, P. Nilsson, J. M. Schwenk, M. Hamsten, K. von Feilitzen, M. Forsberg, L. Persson, F. Johansson, M. Zwahlen, G. von Heijne, J. Nielsen, F. Ponten, Proteomics. Tissue-based map of the human proteome. *Science* **347**, 1260419 (2015).
4. *Tissue Expression of PPARA - Summary - The Human Protein Atlas*, www.proteinatlas.org/ENSG00000186951-PPARA/tissue (2021).
5. S. Kersten, B. Desvergne, W. Wahli, Roles of PPARs in health and disease. *Nature* **405**, 421–424 (2000).
6. H. Keller, C. Dreyer, J. Medin, A. Mahfoudi, K. Ozato, W. Wahli, Fatty acids and retinoids control lipid metabolism through activation of peroxisome proliferator-activated receptor-retinoid X receptor heterodimers. *Proc. Natl. Acad. Sci. U.S.A.* **90**, 2160–2164 (1993).
7. C. Bernal-Mizrachi, S. Weng, C. Feng, B. N. Finck, R. H. Knutsen, T. C. Leone, T. Coleman, R. P. Mecham, D. P. Kelly, C. F. Semenkovich, Dexamethasone induction of hypertension and diabetes is PPAR-alpha dependent in LDL receptor-null mice. *Nat. Med.* **9**, 1069–1075 (2003).
8. A. Warden, J. Truitt, M. Merriman, O. Ponomareva, K. Jameson, L. B. Ferguson, R. D. Mayfield, R. A. Harris, Localization of PPAR isotypes in the adult mouse and human brain. *Sci. Rep.* **6**, 27618 (2016).
9. A. Cimini, E. Benedetti, L. Cristiano, P. Sebastiani, M. A. D'Amico, B. D'Angelo, S. Di Loreto, Expression of peroxisome proliferator-activated receptors (PPARs) and retinoic acid receptors (RXRs) in rat cortical neurons. *Neuroscience* **130**, 325–337 (2005).
10. S. Moreno, S. Farioli-Vecchioli, M. P. Ceru, Immunolocalization of peroxisome proliferator-activated receptors and retinoid X receptors in the adult rat CNS. *Neuroscience* **123**, 131–145 (2004).
11. G. T. Corbett, F. J. Gonzalez, K. Pahan, Activation of peroxisome proliferator-activated receptor α stimulates ADAM10-mediated proteolysis of APP. *Proc. Natl. Acad. Sci. U.S.A.* **112**, 8445–8450 (2015).
12. R. Luo, L. Y. Su, G. Li, J. Yang, Q. Liu, L. X. Yang, D. F. Zhang, H. Zhou, M. Xu, Y. Fan, J. Li, Y. G. Yao, Activation of PPARA-mediated autophagy reduces Alzheimer disease-like pathology and cognitive decline in a murine model. *Autophagy* **16**, 52–69 (2019).
13. A. Roy, M. Jana, G. T. Corbett, S. Ramaswamy, J. H. Kordower, F. J. Gonzalez, K. Pahan, Regulation of cyclic AMP response element binding and hippocampal plasticity-related genes by peroxisome proliferator-activated receptor α. *Cell Rep.* **4**, 724–737 (2013).
14. M. Knobloch, G. A. Pilz, B. Ghesquiere, W. J. Kovacs, T. Wegleiter, D. L. Moore, M. Hruzova, N. Zamboni, P. Carmeliet, S. Jessberger, A fatty acid oxidation-dependent metabolic shift regulates adult neural stem cell activity. *Cell Rep.* **20**, 2144–2155 (2017).
15. M. Maekawa, A. Watanabe, Y. Iwayama, T. Kimura, K. Hamazaki, S. Balan, H. Ohba, Y. Hisano, Y. Nozaki, T. Ohnishi, M. Toyoshima, C. Shimamoto, K. Iwamoto, M. Bundo, N. Osumi, E. Takahashi, A. Takashima, T. Yoshikawa, Polyunsaturated fatty acid deficiency during neurodevelopment in mice models the prodromal state of schizophrenia through epigenetic changes in nuclear receptor genes. *Transl. Psychiatry* **7**, e1229 (2017).
16. M. Costa, A. Squassina, D. Congiu, C. Chillotti, P. Niola, S. Galderisi, M. Pistis, M. Del Zompo, Investigation of endocannabinoid system genes suggests association between peroxisome proliferator activator receptor-α gene (PPARA) and schizophrenia. *Eur. Neuropsychopharmacol.* **23**, 749–759 (2013).
17. G. D'Agostino, C. Cristiano, D. J. Lyons, R. Citraro, E. Russo, C. Avagliano, R. Russo, G. M. Raso, R. Meli, G. De Sarro, L. K. Heisler, A. Calignano, Peroxisome proliferator-activated receptor alpha plays a crucial role in behavioral repetition and cognitive flexibility in mice. *Mol. Metab.* **4**, 528–536 (2015).
18. M. V. Chakravarthy, I. J. Lodhi, L. Yin, R. R. Malapaka, H. E. Xu, J. Turk, C. F. Semenkovich, Identification of a physiologically relevant endogenous ligand for PPARα in liver. *Cell* **138**, 476–488 (2009).
19. S. A. Kliewer, S. S. Sundseth, S. A. Jones, P. J. Brown, G. B. Wisely, C. S. Koble, P. Devchand, W. Wahli, T. M. Willson, J. M. Lenhard, J. M. Lehmann, Fatty acids and eicosanoids regulate gene expression through direct interactions with peroxisome proliferator-activated receptors alpha and gamma. *Proc. Natl. Acad. Sci. U.S.A.* **94**, 4318–4323 (1997).
20. P. R. Devchand, H. Keller, J. M. Peters, M. Vazquez, F. J. Gonzalez, W. Wahli, The PPARα-leukotriene B4 pathway to inflammation control. *Nature* **384**, 39–43 (1996).
21. A. Roy, K. Pahan, PPARα signaling in the hippocampus: Crosstalk between fat and memory. *J. Neuroimmune Pharmacol.* **10**, 30–34 (2015).
22. C. Betsholtz, Lipid transport and human brain development. *Nat. Genet.* **47**, 699–701 (2015).
23. A. Roy, M. Kundu, M. Jana, R. K. Mishra, Y. Yung, C. H. Luan, F. J. Gonzalez, K. Pahan, Identification and characterization of PPARα ligands in the hippocampus. *Nat. Chem. Biol.* **12**, 1075–1083 (2016).
24. P. Campolongo, B. Roozendaal, V. Trezza, V. Cuomo, G. Astarita, J. Fu, J. L. McGaugh, D. Piomelli, Fat-induced satiety factor oleoylethanolamide enhances memory consolidation. *Proc. Natl. Acad. Sci. U.S.A.* **106**, 8027–8031 (2009).
25. R. P. Bazinet, S. Laye, Polyunsaturated fatty acids and their metabolites in brain function and disease. *Nat. Rev. Neurosci.* **15**, 771–785 (2014).
26. R. J. S. Lacombe, R. Chouinard-Watkins, R. P. Bazinet, Brain docosahexaenoic acid uptake and metabolism. *Mol. Aspects Med.* **64**, 109–134 (2018).
27. W. J. Lukiw, J. G. Cui, V. L. Marcheselli, M. Bodker, A. Botkjaer, K. Gotlinger, C. N. Serhan, N. G. Bazan, A role for docosahexaenoic acid-derived neuroprotectin D1 in neural cell survival and Alzheimer disease. *J. Clin. Invest.* **115**, 2774–2783 (2005).
28. M. J. Weiser, C. M. Butt, M. H. Mohajeri, Docosahexaenoic acid and cognition throughout the lifespan. *Nutrients* **8**, 99 (2016).
29. L. Lauritzen, P. Brambilla, A. Mazzocchi, L. B. Harslof, V. Ciappolino, C. Agostoni, DHA effects in brain development and function. *Nutrients* **8**, 6 (2016).
30. S. M. Innis, Dietary (n-3) fatty acids and brain development. *J. Nutr.* **137**, 855–859 (2007).
31. A. J. Richardson, J. R. Burton, R. P. Sewell, T. F. Spreckelsen, P. Montgomery, Docosahexaenoic acid for reading, cognition and behavior in children aged 7-9 years: A randomized, controlled trial (the DOLAB Study). *PLOS ONE* **7**, e43909 (2012).
32. G. Astarita, K. M. Jung, N. C. Berchtold, V. Q. Nguyen, D. L. Gillen, E. Head, C. W. Cotman, D. Piomelli, Deficient liver biosynthesis of docosahexaenoic acid correlates with cognitive impairment in Alzheimer's disease. *PLOS ONE* **5**, e12538 (2010).
33. A. E. Heaton, S. J. Meldrum, J. K. Foster, S. L. Prescott, K. Simmer, Does docosahexaenoic acid supplementation in term infants enhance neurocognitive functioning in infancy? *Front. Hum. Neurosci.* **7**, 774 (2013).
34. S. Meldrum, K. Simmer, Docosahexaenoic acid and neurodevelopmental outcomes of term infants. *Ann. Nutr. Metab.* **69**, 22–28 (2016).
35. J. F. Gould, K. Treyvaud, L. N. Yelland, P. J. Anderson, L. G. Smithers, A. J. McPhee, M. Makrides, Seven-year follow-up of children born to women in a randomized trial of prenatal DHA supplementation. *JAMA* **317**, 1173–1175 (2017).
36. P. B. Derogis, F. P. Freitas, A. S. Marques, D. Cunha, P. P. Appolinario, F. de Paula, T. C. Lourenco, M. Murgu, P. Di Mascio, M. H. Medeiros, S. Miyamoto, The development of a specific and sensitive LC-MS-based method for the detection and quantification of hydroperoxy- and hydroxydocosahexaenoic acids as a tool for lipidomic analysis. *PLOS ONE* **8**, e77561 (2013).
37. S. Naoe, H. Tsugawa, M. Takahashi, K. Ikeda, M. Arita, Characterization of lipid profiles after dietary intake of polyunsaturated fatty acids using integrated untargeted and targeted lipidomics. *Metabolites* **9**, 241 (2019).
38. P. Sapieha, A. Stahl, J. Chen, M. R. Seaward, K. L. Willett, N. M. Krah, R. J. Dennison, K. M. Connor, C. M. Aderman, E. Liclican, A. Carughi, D. Perelman, Y. Kanaoka, J. P. Sangiovanni, K. Gronert, L. E. Smith, 5-Lipoxygenase metabolite 4-HDHA is a mediator of the antiangiogenic effect of omega-3 polyunsaturated fatty acids. *Sci. Transl. Med.* **3**, 69ra12 (2011).
39. S. C. Perry, C. Kalyanaraman, B. E. Tourdot, W. S. Conrad, O. Akinkugbe, J. C. Freedman, M. Holinstat, M. P. Jacobson, T. R. Holman, 15-Lipoxygenase-1 biosynthesis of 7S,14S-diHDHA implicates 15-lipoxygenase-2 in biosynthesis of resolvin D5. *J. Lipid Res.* **61**, 1087–1103 (2020).
40. J. M. Schwab, N. Chiang, M. Arita, C. N. Serhan, Resolvin E1 and protectin D1 activate inflammation-resolution programmes. *Nature* **447**, 869–874 (2007).
41. M. Spite, L. V. Norling, L. Summers, R. Yang, D. Cooper, N. A. Petasis, R. J. Flower, M. Perretti, C. N. Serhan, Resolvin D2 is a potent regulator of leukocytes and controls microbial sepsis. *Nature* **461**, 1287–1291 (2009).
42. H. Y. Kim, J. W. Karanian, T. Shingu, N. Salem Jr., Stereochemical analysis of hydroxylated docosahexaenoates produced by human platelets and rat brain homogenate. *Prostaglandins* **40**, 473–490 (1990).
43. M. Zhang, A. A. Sayyad, A. Dhesi, A. Orellana, Enantioselective synthesis of 7(S)-hydroxydocosahexaenoic acid, a possible endogenous ligand for PPARα. *J. Org. Chem.* **85**, 13621–13629 (2020).
44. K. N. Nina, C. Gonnella, V. S. Martin, K. B. Sharpless, General method for determining absolute configuration of acyclic allylic alcohols. *J. Am. Chem. Soc.* **104**, 3775–3776 (1982).
45. J. Fu, S. Gaetani, F. Oveisi, J. Lo Verme, A. Serrano, F. Rodriguez De Fonseca, A. Rosengarth, H. Luecke, B. Di Giacomo, G. Tarzia, D. Piomelli, Oleylethanolamide regulates feeding and body weight through activation of the nuclear receptor PPAR-α. *Nature* **425**, 90–93 (2003).
46. S. Kamata, T. Oyama, K. Saito, A. Honda, Y. Yamamoto, K. Suda, R. Ishikawa, T. Itoh, Y. Watanabe, T. Shibata, K. Uchida, M. Suematsu, I. Ishii, PPARα ligand-binding domain structures with endogenous fatty acids and fibrates. *iScience* **23**, 101727 (2020).
47. C. Sahin, L. Magomedova, T. A. M. Ferreira, J. Liu, J. Tiefenbach, P. S. Alves, F. J. G. Queiroz, A. S. Oliveira, M. Bhattacharyya, J. Grouleff, P. C. N. Nogueira, E. R. Silveira, D. C. Moreira,

J. Leite, G. D. Brand, D. Uehling, G. Poda, H. Krause, C. L. Cummins, L. A. S. Romeiro, Phenolic lipids derived from cashew nut shell liquid to treat metabolic diseases. *J. Med. Chem.* **65**, 1961–1978 (2022).
48. P. Delerive, C. Furman, E. Teissier, J. Fruchart, P. Duriez, B. Staels, Oxidized phospholipids activate PPARα in a phospholipase A2-dependent manner. *FEBS Lett.* **471**, 34–38 (2000).
49. D. Ma, M. Zhang, C. P. Larsen, F. Xu, W. Hua, T. Yamashima, Y. Mao, L. Zhou, DHA promotes the neuronal differentiation of rat neural stem cells transfected with GPR40 gene. *Brain Res.* **1330**, 1–8 (2010).
50. M. Igarashi, R. A. Santos, S. Cohen-Cory, Impact of maternal n-3 polyunsaturated fatty acid deficiency on dendritic arbor morphology and connectivity of developing Xenopus laevis central neurons in vivo. *J. Neurosci.* **35**, 6079–6092 (2015).
51. H. Cao, M. Y. Li, G. Li, S. J. Li, B. Wen, Y. Lu, X. Yu, Retinoid X receptor α regulates DHA-dependent spinogenesis and functional synapse formation in vivo. *Cell Rep.* **31**, 107649 (2020).
52. G. R. DiResta, J. B. Lee, E. Arbit, Measurement of brain tissue specific gravity using pycnometry. *J. Neurosci. Methods* **39**, 245–251 (1991).
53. M. L. Orozco Morales, C. A. Rinaldi, E. de Jong, S. M. Lansley, J. P. A. Gummer, B. Olasz, S. Nambiar, D. E. Hope, T. H. Casey, Y. C. G. Lee, C. Leslie, G. Nealon, D. M. Shackleford, A. K. Powell, M. Grimaldi, P. Balaguer, R. M. Zemek, A. Bosco, M. J. Piggott, A. Vrielink, R. A. Lake, W. J. Lesterhuis, PPARα and PPARgamma activation is associated with pleural mesothelioma invasion but therapeutic inhibition is ineffective. *iScience* **25**, 103571 (2022).
54. K. Sakimura, T. Kutsuwada, I. Ito, T. Manabe, C. Takayama, E. Kushiya, T. Yagi, S. Aizawa, Y. Inoue, H. Sugiyama, M. Mishina, Reduced hippocampal LTP and spatial learning in mice lacking NMDA receptor epsilon 1 subunit. *Nature* **373**, 151–155 (1995).
55. M. J. Kennedy, M. D. Ehlers, Organelles and trafficking machinery for postsynaptic plasticity. *Annu. Rev. Neurosci.* **29**, 325–362 (2006).
56. H. K. Lee, K. Takamiya, J. S. Han, H. Man, C. H. Kim, G. Rumbaugh, S. Yu, L. Ding, C. He, R. S. Petralia, R. J. Wenthold, M. Gallagher, R. L. Huganir, Phosphorylation of the AMPA receptor GluR1 subunit is required for synaptic plasticity and retention of spatial memory. *Cell* **112**, 631–643 (2003).
57. J. Gerstmeier, M. E. Newcomer, S. Dennhardt, E. Romp, J. Fischer, O. Werz, U. Garscha, 5-Lipoxygenase-activating protein rescues activity of 5-lipoxygenase mutations that delay nuclear membrane association and disrupt product formation. *FASEB J.* **30**, 1892–1900 (2016).
58. M. Fukushima, Biological activities and mechanisms of action of PGJ2 and related compounds: An update. *Prostaglandins Leukot. Essent. Fatty Acids* **47**, 1–12 (1992).
59. M. Furuhashi, G. S. Hotamisligil, Fatty acid-binding proteins: Role in metabolic diseases and potential as drug targets. *Nat. Rev. Drug Discov.* **7**, 489–503 (2008).
60. T. Itoh, L. Fairall, K. Amin, Y. Inaba, A. Szanto, B. L. Balint, L. Nagy, K. Yamamoto, J. W. Schwabe, Structural basis for the activation of PPARgamma by oxidized fatty acids. *Nat. Struct. Mol. Biol.* **15**, 924–931 (2008).
61. A. H. Metherel, R. J. S. Lacombe, J. J. Aristizabal Henao, D. Morin-Rivron, A. P. Kitson, K. E. Hopperton, D. Chalil, M. Masoodi, K. D. Stark, R. P. Bazinet, Two weeks of docosahexaenoic acid (DHA) supplementation increases synthesis-secretion kinetics of n-3 polyunsaturated fatty acids compared to 8 weeks of DHA supplementation. *J. Nutr. Biochem.* **60**, 24–34 (2018).
62. S. J. Iverson, S. L. Lang, M. H. Cooper, Comparison of the Bligh and Dyer and Folch methods for total lipid determination in a broad range of marine tissue. *Lipids* **36**, 1283–1287 (2001).
63. R. A. Colas, M. Shinohara, J. Dalli, N. Chiang, C. N. Serhan, Identification and signature profiles for pro-resolving and inflammatory lipid mediators in human tissue. *Am. J. Physiol. Cell Physiol.* **307**, C39–C54 (2014).
64. P. J. Brown, L. W. Stuart, K. P. Hurley, M. C. Lewis, D. A. Winegar, J. G. Wilson, W. O. Wilkison, O. R. Ittoop, T. M. Willson, Identification of a subtype selective human PPARα agonist through parallel-array synthesis. *Bioorg. Med. Chem. Lett.* **11**, 1225–1227 (2001).

Funding: J.L. was supported by a Charles H. Best Postdoctoral Fellowship and Precision Medicine Initiative (PRiME) Fellowship. C.S. is a recipient of a postgraduate scholarship from the Ministry of National Education, Republic of Turkey. We acknowledge the support from Canadian Institutes of Health Research, instrumentation grants from the Canada Foundation for Innovation, the Ontario Research Fund, and the NSERC Research Tools and Instrument Grant. G.P. acknowledges support from the Ontario Institute for Cancer Research and its funding from the Government of Ontario. The study was supported directly by the following grants: Canadian Institutes of Health Research OME-142884 (to H.M.K.), New Frontiers in Research Fund NFRFE-2019-00901 (to H.M.K., H.P., and C.L.C.), Canadian Institutes of Health Research PJT-156159 (to A.O. and C.L.C.), Canadian Institutes of Health Research FRN-148455 (to L.A.), Canadian Institutes of Health Research MOP119421 and PJT-155959 (to Z.J.), and Natural Science and Engineering Research Council of Canada RGPIN-341498 and RGPIN-2017-06295 (to Z.J.). **Author contributions:** Study conceptualization was done by H.M.K., C.L.C., Z.J., and L.A. Methodology was developed by J.L. and H.P. Investigations were performed by J.L., C.S., L.M., M.Z., A.H.M., and G.P. Visualization was done by S.A. Supervision was provided by H.M.K., H.P., C.L.C., L.A., A.O., and R.P.B. The manuscript was written by J.L. and revised and edited by H.M.K. and C.L.C. **Competing interests:** The authors declare that they have no competing interests. **Data and materials availability:** Metabolomic data are publicly available in MassIVE, under dataset identifier MSV000085183. All other data needed to evaluate the conclusions in the paper are present in the paper or the Supplementary Materials.

Submitted 19 January 2022
Accepted 13 June 2022
Published 5 July 2022
10.1126/scisignal.abo1857